Pressure Evolution and Production Performance of Waterflooding in *n*-Heptane-Saturated Fired Berea Cores

N. Rezaei and **A. Firoozabadi,** SPE, Reservoir Engineering Research Institute

Summary

This work presents experimental results and interpretation of injection pressure and recovery performance of waterflooding in strongly water-wet fired Berea cores saturated with *n*-heptane. The experiments were conducted at constant injection rate at room conditions, and the effects of injection rate and initial water saturation on the oil-recovery performance and dynamic-injection pressure were investigated. Elements of surprise were observed in the injection-pressure data. The pressure profiles showed four distinct regimes, each governed by capillary or viscous forces. At low capillary numbers ($Ca=u\mu/\sigma<10^{-6}$), capillarity governed two pressure regimes, corresponding to the core inlet and outlet. In the early part of waterflooding, pressure stayed constant for a considerable time before hydrodynamic pressure gradient could overcome the capillary pressure gradient. After viscous forces dominated, a linear increase in injection pressure over time was observed up to breakthrough time. A sudden pressure rise was observed close to breakthrough because of capillary retention at the core outlet. The pressure became constant after the breakthrough when the water- and oil-saturation distributions were stabilized. Changing the injection rate by an order of magnitude in the range from 2.2 to 22.2 pore volumes (PV)/D (equivalent to $Ca=10^{-7}$ to 10^{-6}) did not appreciably change the oil-recovery performance; similar breakthrough time and final oil recovery were observed. The effect of initial water saturation was also investigated. When lowering the initial water saturation beyond that established in oil flooding, production performance and injection pressure were similar to those of a core without the initial water saturation. The injection pressure at breakthrough was found to decrease with increase of the initial water saturation. Waterflooding was modeled by including the capillary pressure and excellent agreement was obtained with experimental results of production and injection pressure. We find that in the absence of in-situ saturation measurements, the injection pressure is a better variable for tuning the model parameters compared with the production history alone.

Introduction

Waterflooding has been applied for oil recovery since 1880 when Carll (1880) proposed the idea for the first time. This process has been the subject of extensive research. Experimental and mathematical modeling aspects of waterflooding are investigated both at the macro- and the microscale (the latter to a lesser extent). In a macroscale perspective, waterflooding experiments are designed to investigate the effect of initial water saturation (Brown 1957; Kelley and Caudle 1966; Tang and Morrow 1997; Zhou et al. 2000; Tang and Firoozabadi 2001; Zhang et al. 2007), injection rate (Rapoport and Leas 1953; Kyte and Rapoport 1958; Abrams 1975; Chatzis et al. 1983; Jadhunandan and Morrow 1995; Zhou et al. 1995; Tang and Firoozabadi 2001; Mai and Kantzas 2009; Torabi et al. 2010), wettability (Kennedy et al. 1955; Morrow et al. 1986; Anderson 1987a, b; Jadhunandan and Morrow 1995; Yildiz et al. 1999; Zhou et al. 2000; Agbalaka et al. 2008; Ashraf et al. 2010; Wu et al. 2011), permeability heterogeneity (Hamon and Vidal 1986; Dawe et al. 1992; Gharbi and Peters 1993; Catalan et al. 1994; Huang et al. 1996; Oseto et al. 2006; Chalbaud et al. 2007; Zhou et al. 2008; Yu et al. 2009; Parsaei and Chatzis 2011), salinity (Bernard 1967; Yildiz and Morrow 1996; Tang and Morrow 1997; Yildiz et al. 1999; Zhou et al. 2000; Sharma and Filoco 2000; Tie et al. 2003; Lager et al. 2007; Zhang et al. 2007; Ashraf et al. 2010), temperature (Edmondson 1965; Zhou et al. 1995; Tang and Morrow 1997; Morrow et al. 1998; Zhou et al. 2000; Hognesen et al. 2005), fluid viscosity (Rapoport and Leas 1953; Fried 1954; Kyte and Rapoport 1958; Mungan 1971; Abrams 1975; Ju et al. 2006; Mai and Kantzas 2009; Wang and Dong 2009), and oil composition (Jadhunandan and Morrow 1995; Tang and Morrow 1997; Buckley and Liu 1998; Morrow et al. 1998).

Although there has been extensive research on waterflooding, the analysis of pressure data in coreflooding—despite its importance—is surprisingly overlooked in the literature. Injection pressure is more sensitive to the wetting-phase-saturation distribution compared with the oil-recovery history because of the strong influence of saturation distribution on the mobility of each phase. Therefore, in the absence of in-situ saturation measurements, the injection pressure can be included in addition to production history to tune the mathematical model that describes the flow process. The outcome from this model can be saturation distribution, or relative permeability and capillary pressure functions. The objective of this work is to study the dynamic pressure evolution and the oil-recovery performance in waterflooding in strongly water-wet fired Berea cores. The effects of injection rate and connate-water saturation on pressure evolution and recovery performance are investigated in the *n*-C_7/brine system. We use a mathematical model that includes capillarity to analyze pressure and recovery data.

Experiments

Test Fluids. CO_2 and N_2 gases, *n*-heptane (Macron Chemicals, 99.0%), purified water, and two different brines were used in the waterflooding experiments. Density, viscosity, and surface tension of the oil and brine phases and the pH of both brines at room conditions are shown in **Table 1.** The viscosities of fluids were measured by capillary viscometers (Cannon-Fenske, No. 25, 100 and 200); the densities were measured by pycnometers (10 cm^3 Gay-Lussac, Wilmad-LabGlass); and the surface tensions were measured by plate tensiometer (K12 Processor Tensiometer, Krüss). Fluid-characterization tests were conducted in an isothermal water bath of 25°C. The compositions of brines are shown in **Table 2.** Different solvents, such as methanol (Cole-Parmer, 98.8%), isopropyl alcohol (IPA) (Cole-Parmer, 99.5%), and methylene chloride (Fisher Scientific, 99.9%), were used in the core cleaning.

In Table 1, μ, ρ, and σ are viscosity, density, and surface tension of fluids, respectively.

Core Characteristics. The Berea sandstone cores were obtained from Cleveland quarries with porosities of 18.9 to 22.8% and initial absolute permeability to brine (K_w^0)of 141 to 637 md. **Table 3** lists the properties of the cores. In this table, T_f is the temperature at which the cores are fired; L and D are the length and diameter of the cores, respectively; PV and ϕ are the total effective pore volume (PV) and porosity of the cores, respectively; and K_w^0 is initial absolute permeability of the core to brine. Cores B4F, B5F, and B8F were fired at a temperature of 1000°C, and Core B2F was fired

Original manuscript received for review 6 February 2013. Revised manuscript received for review 2 July 2013. Paper (SPE 167264) peer approved 11 September 2013.

TABLE 1—PHYSICAL PROPERTIES OF OIL AND BRINE AT ROOM TEMPERATURE (25°C)

		Physical Property			
Phase	Fluid	μ (cp)	ρ (g/cm^3)	σ (mN/m)	pH
Brine	Brine Q	1.031 ± 0.002	1.008 ± 0.002	72.78 ± 0.38	6.78 ± 0.01
	Brine C	0.996 ± 0.001	1.000 ± 0.003	62.55 ± 0.35	6.70 ± 0.01
Oil	n-C_7	0.420 ± 0.001	0.684 ± 0.000	19.95 ± 0.05	n/a

TABLE 2—CONCENTRATION OF SALTS FOR TWO BRINES

	Salt Concentration (ppm)	
Ion	Brine Q	Brine C
NaCl	28,390	—
KCl	3,051	—
$CaCl_2$	7,000	3,000
$MgCl_2$	3,510	—

at 600°C. During the firing, the temperature of the oven was gradually increased (in approximately 5 hours) to avoid thermal shock to the cores, as suggested by Wu and Firoozabadi (2011). We fired the cores to stabilize the clay and to avoid the clay swelling interfering with the pressure data. Considerable increases in the core porosity and bulk density were observed from firing. Cores B4F, B5F, and B8F were obtained from the same batch and exhibited similar petrophysical properties, different from those of Core B2F. Core B2F was used for a porosimetry experiment to detect the inlet and outlet dead volumes by use of the constant-rate-air-injection method (Smith et al. 2005; Rezaei and Chatzis 2011).

Fig. 1 shows the pore-scale views (with KEYENCE VHX 2000 microscope) of Berea core before and after firing. The figure shows that the firing at a temperature of 1000°C significantly changes the pore structure. For example, pore throats are enlarged, the pore interconnectivity is enhanced, and grain surfaces are partially melted, resulting in decreased surface roughness. The macroscopic significance of firing is an increase in oil recovery (Shaw et al. 1991; Ma and Morrow 1994), which is also observed in this work.

The fired cores were initially washed with several PV of methylene chloride, brine C, IPA , and methanol, and dried overnight in a convection oven at a temperature of 150°C before waterflooding experiments. The core bulk volume was geometrically measured through average core diameter and length. Saturation method was used to measure the effective porosity of the cores, following a protocol suggested by Worthington (1978). The cores were first covered by several layers of Kimwipes to avoid desaturation during the core handling, and they were placed in a saturation vessel. Vacuum of 6.7 Pa (50 mTorr) was applied to the saturation vessel for a period of 6 hours. Deaerated Brine C (filtered to 60 μm) was injected into the core and pressurized to 6.2 MPa for 16 hours. The vacuum was applied to the core by a mechanical pump, by use of an inline cold trap of −86°C. The porosity was calculated by the increase in the weight of dry cores, with the core bulk volumes. After the porosity measurement, the cores were covered by Teflon heat-shrink tubes to improve their mechanical strength for permeability and waterflooding experiments. The fired cores were handled with care because the core cement materials can be

TABLE 3—CHARACTERISTICS OF BEREA SANDSTONE CORES AFTER FIRING

		Dimensions (cm)				
Core	T_f (°C)	L	D	PV* (mL)	ϕ (% PV)	K_w^0 (md)
B2F	600	17.92	3.87	39.8	18.9	141
B4F	1000	26.36	3.77	64.8	22.5	570
B5F	1000	25.56	3.76	64.8	22.8	597
B8F	1000	25.60	3.75	64.0	22.7	637

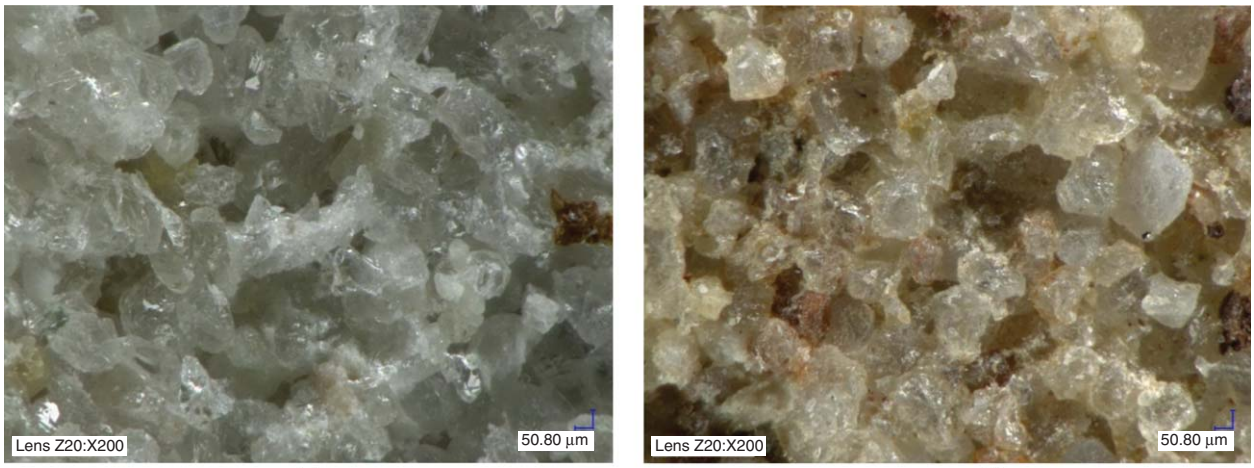

(a) (b)

Fig. 1—Pore-scale view of Berea core for (a) unfired and (b) fired cores.

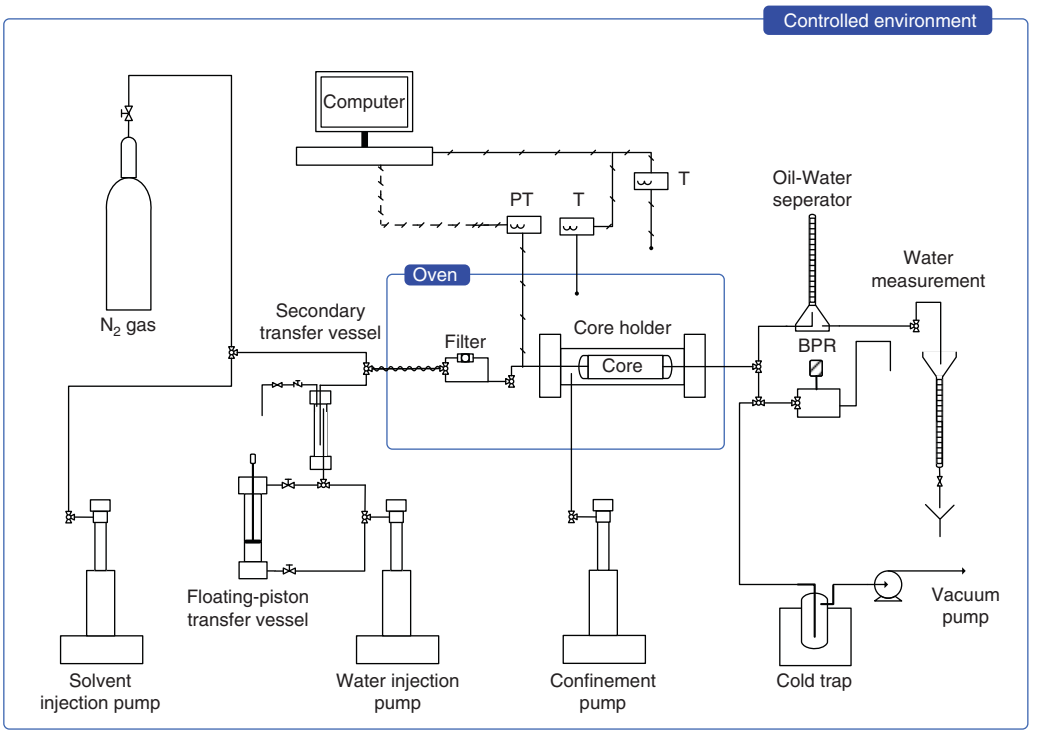

Fig. 2—Experimental setup for waterflooding experiments.

destructed in firing (Wu and Firoozabadi 2011), and the fired cores can consequently lose their mechanical strength. The grain particles may easily cut off upon an applied shear. The Teflon layer significantly helps to avoid shearing the core outer surface. Still, the injecting fluids can shear the core pore structure, so the use of high injection rates should be avoided in the fired cores.

In our early experiments of porosity and permeability measurements, CO_2 was used to miscibly displace the air in the core. CO_2 is heavier than the air, which can be later dissolved into the brine (or oil), if trapped; however, we experienced incomplete saturation and severe permeability reduction. We abandoned the use of CO_2. The reversible chain of reactions between CO_2, H_2O, CaO, and $CaCO_3$ (Huggett 2007) may result in calcite precipitates, which eventually plug the core; the presence of Ca^{2+} ions in the brine ($CaCl_2$) also adds to the complexity. During the firing process, the calcite ($CaCO_3$) will convert to CaO and will release CO_2 (Wu and Firoozabadi 2011):

$$CaCO_3(s) \xrightarrow{\Delta} CaO(s) \downarrow + CO_2(g) \uparrow . \quad \ldots\ldots\ldots\ldots (1)$$

CaO can react again, in the presence of H_2O and CO_2, in an exothermic reaction (Atkins and Jones 2007):

$$CaO(s) + H_2O(l) \rightarrow Ca^{2+}(aq) + 2OH^{-}(aq). \quad \ldots\ldots\ldots (2)$$

Calcium hydroxide can react with CO_2 to precipitate calcite:

$$Ca(OH)_2(aq) + CO_2(g) \rightarrow CaCO_3(s) \downarrow + H_2O(l). \quad \ldots\ldots (3)$$

The precipitation of calcite may cause core plugging. On the other hand, the addition of CO_2 may cause a portion of precipitated calcite to redissolve into the aqueous phase (Boynton 1980; Huggett 2007):

$$CaCO_3(s) + CO_2(g) + H_2O(l) \rightarrow Ca^{2+}(aq) + 2(HCO_3)^{-}(aq). \quad \ldots\ldots\ldots\ldots\ldots\ldots (4)$$

Experimental Setup and Methodology. A schematic of waterflooding experiments is depicted in **Fig. 2.** The main elements of this setup are: Isco pumps for the delivery of water (both injecting and confining) and cleaning solvents (during core cleanup), a Hassler core holder, isothermal oven, floating-piston and secondary transfer vessels, water/oil separator, vacuum pump and cold trap, high-pressure gas cylinders, backpressure regulator, and instrumentation and data acquisition system.

The core holder was placed horizontally in a convection oven with controlled temperature. The experimental setup was also maintained in a controlled environment to avoid temperature difference between the core-holder assembly and the separation column. The core outflow from the waterflooding and permeability tests was drained to an atmospheric separator; the outlet pressure was fixed at zero (gauge). The pressure of injecting brine and the temperature of the oven, as well as the controlled environment, were recorded. The pumps were connected to their supply liquids through a 60-μm inline filter to avoid possible solid contaminations. Another 60-μm filter was installed at the core inlet to prevent intrusion of fine particles into the core. This filter was used only during the liquid saturation and during the cleaning procedures; the filter was bypassed during waterflooding and permeability measurements (to avoid interfering with pressure measurements). A backpressure regulator was used during the saturation and cleanup processes; this filter was bypassed during the waterflooding or permeability tests. We used a dual-transfer-vessel system for liquid delivery to ensure a complete liquid saturation. The second transfer vessel was added to the conventional coreflooding setup, allowing the accumulation of any free-gas phase (forms when vacuum was connected to the first transfer vessel) at the top of this vessel, as the liquid was being injected to the core from the bottom section. The outlet relief tubing with a check valve allowed removing the free gas just before the liquid-pressurization stage. Overall, this secondary transfer vessel made the saturation stage safe and robust. At the end of waterflood tests, we continued water injection at higher injection rates (two to three times the waterflood rate) to make sure that the residual oil saturation (ROS) is fully established. There was very little oil production from the increased injection rate.

We have performed a total of nine waterflooding experiments. Six were conducted without the initial water saturation. For these experiments, a single cleaned (and dried) core was used. To

saturate the core with liquids, vacuum of 20 to 50 mTorr was applied. This vacuum line was connected to the vacuum pump through a cold trap to avoid water and solvent vapor diffusing into the vacuum pump. After the core was evacuated to the desired vacuum level for approximately 2 hours, we closed the outlet valve and injected deaerated liquids into it. Just before pressurizing the core, the secondary transfer vessel was drained through a check valve (as the core inlet valve was closed), removing any accumulated gas phase from this vessel. When the system reached a pressure of approximately 20 psig, we opened the core outlet valve to the backpressure-regulator line. The pressure regulator was adjusted to allow approximately 200-psig backpressure. Then, we flowed approximately 1 to 2 PV of liquids during the backpressure. The liquid (either brine or n-C_7) was allowed to age the core for approximately 12 hours at room conditions. Absolute permeability to liquid was measured after the aging, and then the waterflooding experiment was started by injecting water at constant rate. At the end of the waterflooding experiment (when ROS is achieved), the endpoint relative permeability to brine was measured. Finally, a cleanup procedure was followed by injecting 2 PV of methylene chloride, 5 PV of IPA, and 2 PV of methanol, and flowing high-pressure N_2 through the model. The core was oven dried overnight at 150°C.

Three runs were conducted with initial water saturation; the core was initially saturated with brine. After measuring the absolute permeability to brine, the core was placed vertically and flooded with oil from th e top, producing brine from the bottom. During the oilflooding, a high level of initial water saturation (approximately 0.44 PV) was established in the core. To lower the initial water saturations, the temperature of the oven containing the core holder was raised to 100°C. With a check valve installed at the core outlet and connecting the inlet to an oil-supply vessel, we vaporized a portion of water in the core without allowing the intrusion of air into it. The core was then flooded with n-C_7, pressurized to 200 psig, and aged overnight to ensure a full liquid saturation. It was then flooded with 1 PV of n-C_7, and we measured the permeability to oil at initial water saturation. We attempted to reduce the initial water saturation by flooding the core with a more-viscous oil (vacuum-pump oil with viscosity of 120 cp), but the oil altered the core wettability. The rest of the procedure steps were similar to the runs with no initial water saturation.

Mathematical Model

Immiscible displacement of water/oil has been modeled for spontaneous imbibition (Pooladi-Darvish and Firoozabadi 2000; Kashchiev and Firoozabadi 2003; Ruth et al. 2007) and forced imbibition (waterflooding) by use of different analytical (Yortsos and Fokas 1983; Ruth and Arthur 2011), numerical, and mechanistic (Chatzis and Dullien 1983; Dong and Dullien 1997; Dong et al. 1998; Dong et al. 2006) models. There are only a few analytical models of waterflooding (Yortsos and Fokas 1983; Ruth and Arthur 2011) available, which are limited to semi-infinite models of a domain for which certain capillary pressure function and viscous terms are assumed in the governing equation. Numerical simulations are usually used to model waterflooding (Douglas et al. 1958; Kyte and Rapoport 1958). Here, we use the theoretical framework proposed by Whitaker (1986) in the form of a frontal advanced model with capillary pressure effects.

Governing Equations. The mathematical model of waterflooding can be constructed by a set of equations containing the continuity of each phase (oil or water), total mass conservation, and momentum conservation (Darcy's law) (Whitaker 1986).

Continuity equation for phase α (oil or water),

$$-\nabla(\rho_\alpha u_\alpha) = \frac{\partial}{\partial t}(\rho_\alpha S_\alpha \phi), \alpha = w, o \quad \ldots\ldots\ldots\ldots\ldots (5)$$

where ρ_α, S_α, and u_α are density, saturation, and superficial velocity, respectively, for phase α; ϕ is the porosity of medium; and t is time.

Generalized Darcy's law velocity for phase α is

$$u_\alpha = -\frac{Kk_{r\alpha}}{\mu_\alpha}(\nabla P_\alpha - \rho_\alpha g), \alpha = w, o, \quad \ldots\ldots\ldots\ldots\ldots (6)$$

where K is the absolute permeability of media; $k_{r\alpha}$, P_α, and μ_α, are relative permeability, pressure, and viscosity of phase α, respectively; and g is gravitational-acceleration constant.

The expression for the total flow rate is given by

$$q_t = \sum_\alpha q_\alpha = \sum_\alpha \left[-\frac{AKk_{r\alpha}}{\mu_\alpha}(\nabla P_\alpha - \rho_\alpha g)\right], \alpha = w, o, \quad \ldots\ldots\ldots\ldots\ldots (7)$$

where q_t and q_α are total injection rate and flow rate of phase α, respectively, and A is the core cross-sectional area.

To obtain an explicit equation in terms of water saturation, the following assumptions were made:

- Fluid and core compressibilities are negligible.
- Flow is unidirectional (horizontal), and the gravity effects are neglected.
- Core is homogeneous and strongly hydrophilic.
- Capillary equilibrium holds.
- There are only two immiscible phases: oil and water.

With Eqs. 5 through 7 and these assumptions, the following dimensionless equation can describe the wetting-phase saturation (S_D) as a function of spatial coordinate (x_D) and time (t_D):

$$\eta \frac{\partial S_D}{\partial t_D} = \frac{\partial}{\partial x_D}\left[\lambda_{rw}\left(1 + \zeta_o \frac{\partial S_D}{\partial x_D}\right)\right]. \quad \ldots\ldots\ldots\ldots\ldots (8)$$

In Eq. 8, S_D, x_D, and t_D are normalized saturation, length, and time, respectively. Six dimensionless numbers were involved in Eq. 8 and are defined as

$$\begin{aligned} x_D &= \frac{x}{L} \\ S_D &= \frac{S_w - S_{wi}}{1 - S_{wi} - S_{or}} \\ t_D &= \frac{tq_t}{AL\phi} \\ \eta &= -(1 - S_{wi} - S_{or}) \\ \lambda_{rw} &= \frac{1}{1 + \left(\frac{k_{ro}}{k_{rw}}\right)\left(\frac{\mu_w}{\mu_o}\right)} \\ \zeta_o &= \frac{AK\left(\frac{k_{ro}}{\mu_o}\right)}{Lq_t}\frac{dP_c}{dS_D} \end{aligned}, \quad \ldots\ldots\ldots\ldots\ldots (9)$$

where L is the core length; S_w, S_{wi}, and S_{or} are saturation of water, initial saturation of water, and residual oil saturation, respectively; t and x are time and location, respectively; μ_w and μ_o are the viscosity of water and oil, respectively; P_c is capillary pressure; and k_{rw} and k_{ro} are water and oil relative permeabilities, respectively.

The initial condition is

$$S_D(0, x_D) = 0. \quad \ldots\ldots\ldots\ldots\ldots (10)$$

Regarding the boundary conditions, at $x_D = 0$, there is no inflow of oil at times $t_D > 0$. This boundary condition is not valid when the oil/water interface first reaches the core inlet ($t_D \approx 0$) because the oil at the inlet-face pore spaces will be initially removed by imbibition of water at $x_D = 0$. However, this initial time is insignificant compared with the process time scale, so $q_t = q_w$,

$$\left(\frac{\partial S_D}{\partial x_D}\right)_{x_D=0} = \left(\frac{1}{\zeta_w}\right)_{x_D=0}, \; t_D > 0, \quad \ldots\ldots\ldots\ldots\ldots (11)$$

where ζ_w is a dimensionless number similar to ζ_o (defined in Eq. 9), with the exception that the term for mobility of oil is replaced

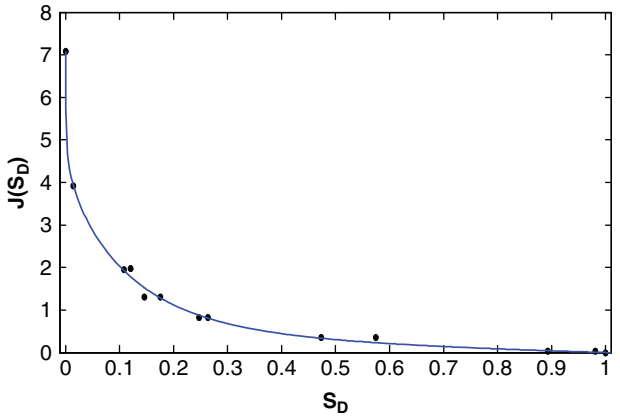

Fig. 3—Leverett *J*-function for Berea core defined in Eq. 16 along with imbibition capillary pressure data obtained from porous-plate method (Bolås and Torsaeter 1995).

by that for mobility of water. The boundary condition at the core outflow is more complicated. At $x_D = 1$, the boundary condition changes before and after water breakthrough. Before water reaches the core outflow face, there is no flow of water out of the core (if initial water is immobile). Alternatively, the oil pressure before breakthrough is described by upstream backpressure whereas the pressure of water at core outlet face is described by capillary pressure at initial water saturation. When water reaches the core outlet face, it accumulates there before leaving the core because of the discontinuity in the capillary pressure. This phenomenon is defined by the terms capillary retention or capillary end effect. The boundary condition at exit before breakthrough can be written as $q_t = q_o$, or

$$\left(\frac{\partial S_D}{\partial x_D}\right)_{x_D=1} = \left(\frac{-1}{\zeta_o}\right)_{x_D=1}. \quad \ldots\ldots\ldots\ldots\ldots\ldots (12)$$

In other words, the gradient of capillary pressure and that of the oil phase are equal at the core outlet face, before breakthrough. If the core is strongly water-wet, water accumulates at the core outlet face to reduce the capillary pressure and to enable water production. At ROS conditions, the capillary pressure becomes zero and the pressure of water approaches that of the oil phase. Alternatively, the water saturation stays at ROS after breakthrough. Therefore, during the waterflooding in a strongly water-wet core, negligible oil is produced from the pore spaces of the core outlet face after breakthrough:

$$S_D(t_D, 1) = 1. \quad \ldots\ldots\ldots\ldots\ldots\ldots\ldots\ldots (13)$$

Auxiliary Correlations. Relative permeability and imbibition capillary pressure models define the two-phase flow. We used the relative permeability functions for water and oil proposed by Hirasaki (1975),

$$k_{rw}(S_D) = k^0_{rw} S_D n^w, \quad \ldots\ldots\ldots\ldots\ldots\ldots\ldots (14)$$

$$k_{ro}(S_D) = k^0_{ro}(1 - S_D)^{n_o}, \quad \ldots\ldots\ldots\ldots\ldots\ldots\ldots (15)$$

where the parameters k^0_{rw} and k^0_{ro} are the endpoint relative permeability values of water and oil phases, respectively, which can be measured. The parameters n_w and n_o are the water and oil exponents, respectively. We tuned the relative permeability parameters with the experimental results of injection pressure and production history.

For the imbibition capillary pressure, we fitted a three-parameter model to the experimental data of Bolås and Torsæster (1995), as will be shown in Eq. 16. Imbibition and drainage capillary pressures were measured by Bolås and Torsæster by porous plate and centrifuge methods by use of Exxsol D60/brine fluids in Berea cores with petrophysical properties similar to ours. Here, we use only the experimental imbibition capillary pressure data obtained by the porous-plate method. The following Leverett *J*-function (Leverett 1940) was used:

$$J(S_D) = \frac{P^{\text{imb}}_c(S_D)}{\gamma_{ow}\cos\theta_{ow}}\sqrt{\frac{K}{\phi}} = ae^{(bS_D)} + c\ln(S_D), \quad \ldots\ldots\ldots (16)$$

where γ_{ow} and θ_{ow} are the oil/water interfacial tension and contact angle, respectively, and P^{imb}_c is the imbibition capillary pressure. The Leverett *J*-function defined in Eq. 16 is plotted in **Fig. 3** along with the experimental data of imbibition (Bolås and Torsaeter 1995). In general, a shift in the capillary pressure curve is expected after firing, but without experimental data for fired cores, we use the same results for our cores.

The Levenberg-Marquardt algorithm was used to fit the three parameters in Eq. 16 to the experimental data; the optimized values are $a = 2.632 \pm 0.447$; $b = -8.127 \pm 1.052$, and $c = -0.3747 \pm 0.0465$. These values were obtained by applying the core permeability and porosity values of 450 md and 24.3% PV, respectively (Bolås and Torsaeter 1995). We used the experimental data of waterflooding to optimize the parameters in the relative permeability model.

The parabolic initial-boundary-value partial-differential equation (Eq. 8) defined the saturation of wetting phase in one spatial coordinate and time, which was coupled with auxiliary correlations (Eqs. 14 through 16); the initial and boundary conditions (Eqs. 10 through 13) were applied to this set of equations. The solver discretized the saturation along the spatial coordinate and integrated it with time.

Results and Discussion

Experimental Results. Nine waterflooding experiments were conducted in three fired Berea cores—B4F, B5F, and B8F—for which a summary of waterflooding recovery results is provided in **Table 4.** We show recovery factor at breakthrough (RF_{BKT}),

TABLE 4—SUMMARY OF WATERFLOODING RESULTS USING *n*-C_7/BRINE Q FLUID PAIR AT DIFFERENT INJECTION RATES

Run	Core	*K* (md)	Q_{inj} PV/D	Q_{inj} cm³/min	S_{wi} (PV)	S_{oi} (PV)	RF_{BKT} (Hydrocarbon PV)	RF_{Sor} (Hydrocarbon PV)	S_{or} (PV)	S_{or}/S_{oi}
1	B4F	551	2.2	0.1	0	1	0.557	0.563	0.437	0.437
2	B4F	398	4.4	0.2	0	1	0.564	0.569	0.431	0.431
3	B4F	396	4.4	0.2	0	1	0.556	0.560	0.440	0.440
4	B4F	390	11.1	0.5	0	1	0.551	0.562	0.438	0.438
5	B4F	480	22.2	1.0	0	1	0.558	0.561	0.439	0.439
6	B8F	495	4.4	0.2	0	1	0.563	0.565	0.435	0.435
7	B5F	575	4.4	0.2	0.438	0.562	0.486	0.486	0.289	0.514
8	B8F	635	4.4	0.2	0.289	0.711	0.562	0.569	0.306	0.430
9	B4F	306	4.4	0.2	0.201	0.799	0.550	0.554	0.356	0.446

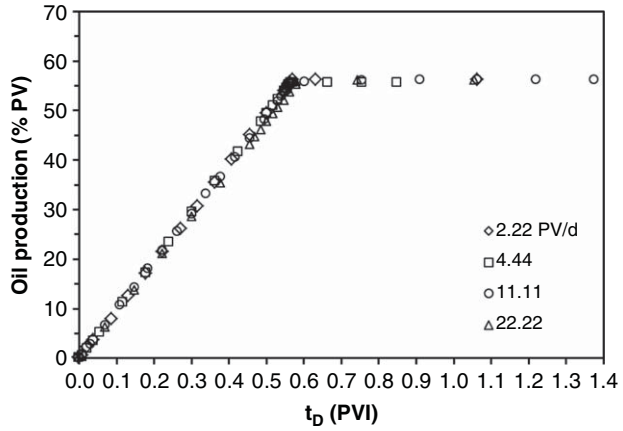

Fig. 4—Oil recovery vs. dimensionless time (PVI) during waterflooding of *n*-C_7-saturated cores for four different injection rates at 25°C.

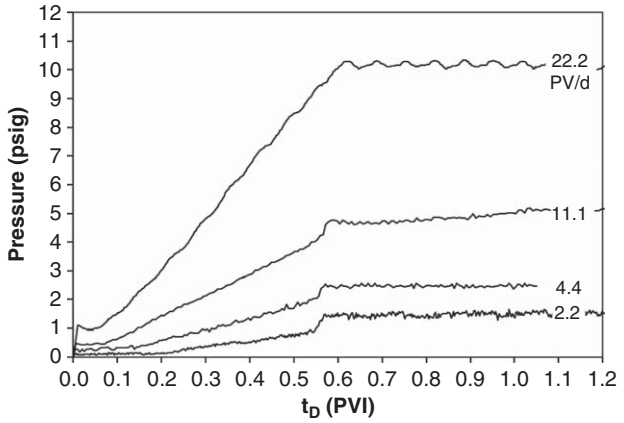

Fig. 5—Injection pressure vs. dimensionless time (PVI) in waterflooding of *n*-C_7-saturated cores for four different flow rates conducted at 25°C. The outlet pressure is atmospheric.

recovery factor at ROS (RF_{Sor}), and S_{or} as the variables illustrating macroscopic recovery performance. All the experiments investigating the effect of injection rate (Runs 1 through 5) were conducted in the same core, B4F. Runs 7 through 9 were conducted with the initial water saturation, and the results were compared with tests without the initial water saturation.

Without Initial Water. Six waterflooding experiments (Runs 2 and 3 are replicates) were conducted without the initial water saturation, as summarized in Table 4. We present the oil-recovery history and the injection-pressure dynamics in **Figs. 4 and 5,** respectively, for four injection rates. As observed in Fig. 4, we did not observe a considerable change in the oil-recovery performance by changing the injection rate in the range of 2.2 to 22.2 PV/D (corresponding to $Ca = 10^{-7}$ to 10^{-6}). The breakthrough time occurred consistently after approximately 0.551 to 0.564 total PV injected (PVI), and the final recovery factor was in the range 0.560 to 0.569 PV, resulting in ROS of 0.431 to 0.440 PV. Because the cores were strongly hydrophilic, little oil was produced after water breakthrough, as observed in the recovery plots. These results are in agreement with observations by Tang and Firoozabadi (2001) on the effect of pressure gradient in strongly water-wet cores. In some of our waterflooding experiments, the tests were allowed to proceed longer (up to 5 PV), but no oil production was observed after the breakthrough.

The brine-injection pressure was measured during the waterflooding tests, as shown in Fig. 5. In all experiments, the pressure of effluent was atmospheric. The core was initially at atmospheric-pressure condition as well. Several elements of surprise were observed in the pressure data. Four distinct pressure regimes were distinguished in Fig. 5. Initially, there was a time period during which the pressure was constant. This region was extended over a longer period of time at the lower injection rates. As observed in Fig. 5, at the injection rate of 2.22 PV/D, approximately 22% PV of brine was injected into the core before the injection pressure started to rise. In the second pressure regime, a linear increase in pressure with time was observed up to water breakthrough. Just before breakthrough, the third regime was observed, featuring a sudden increase in injection pressure. Finally, the pressure stabilized after breakthrough.

These four pressure regimes are shown in **Fig. 6** for waterflooding of Core B2F at 2.72 PV/D, by use of deionized water/*n*-C_7 fluids, and are discussed below.

Regime I. As shown in Fig. 6, approximately 12.5% PV water was injected into the B2F core at 2.72 PV/D before pressure increased. Note that the viscosity of water is higher than that of the oil (*n*-C_7) by a factor of approximately 2.5. We expected the injection pressure to linearly increase over time, from zero to pressure at breakthrough. However, a significant amount of water was injected into the core before detecting an increase in pressure. We measured the inlet dead volume from the volume of inlet tube and connections and, alternatively, from constant-rate-air-injection porosimetry (Rezaei and Chatzis 2011) to be 1.2% PV for this specific core. Therefore, this constant-pressure behavior in Regime I was not associated with the inlet dead volume, and it was explained by the spontaneous water imbibition at the core inlet. In other words, the water imbibed into the continuum of small pores with high capillary pressure, in the direction of reducing the capillary pressure gradient. As the water saturation in the core increased, the viscous pressure drop also increased because water is the more viscous phase. On the other hand, the smaller pores were invaded first and larger pores with smaller capillary pressures became hierarchically invaded as the imbibition proceeded. An increase in the injection pressure can be observed after viscous forces overcome the capillary forces. The contribution of capillary forces during a waterflood is discussed by different authors (Perkins 1957; Melrose and Melrose 1974; Morrow 1979; Chatzis et al. 1983; Chatzis and Morrow 1984; Chatzis et al. 1988; Dawe et al. 1992; McDougall and Sorbie 1993; Hirasaki 1996; Dong et al. 1998; Dullien and Dong 2002; Dong et al. 2006). However, the pressure behavior exhibited in Region I has not been reported in the past, to the best of our knowledge.

As observed in Fig. 5, when the injection rate increased from 2.2 to 22.2 PV/D, the duration of constant pressure decreased from 0.22 PVI to approximately 0.06 PVI. At higher injection rates, the viscous pressure drop is also larger. Therefore, the contribution of capillary pressure in the net pressure drop across the core will be smaller, which results in an earlier core pressurizing. Note that in this pressure regime, the flow behavior is not piston-

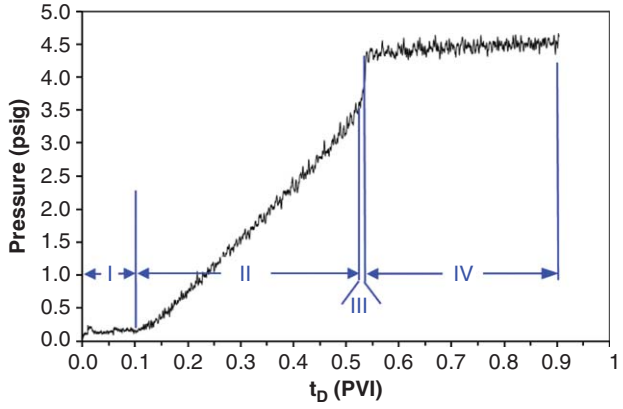

Fig. 6—Injection pressure vs. PVI of deionized water in waterflooding of *n*-C_7-saturated Core B2F for 2.72 PV/D conducted at 25°C.

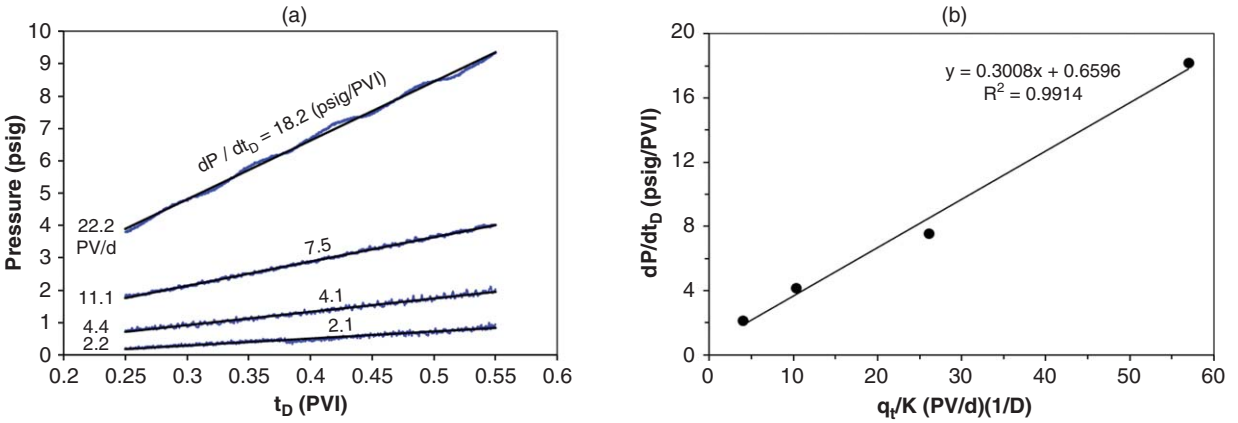

Fig. 7—Plots of (a) linear pressure increase from injection and (b) correlation between rate of pressure increase vs. scaled injection rate. The tests were conducted without initial water saturation.

like, and the water/oil interfaces advance in the direction of reducing the gradient of capillary pressure.

Regime II. The net pressure drop across the core is dominated by the viscous pressure drop in this pressure regime. The injection pressure linearly increased with time, and the slope of increase in pressure over time was found to increase with the injection rate. Because waterflooding was conducted at constant injection rate, the linear trend of pressure increase over time was expected. **Fig. 7a** shows the linear trends of pressure over time during 0.25 to 0.55 PVI (where the core inlet and outlet capillary end effects are negligible at all injection rates) for injection rates of 2.2 to 22.2 PV/D (Fig. 5). The rate of pressure increase by water injection correlates well with the injection rate and permeability of the core, as shown in Fig. 7b. The injection rate on the *x*-axis is in PV/D, and the permeability is in darcies. Although a single core was used for these experiments, a variation in the permeability from 570 to 390 md was observed during the experiments. We included the effect of permeability change in Fig. 7b by scaling the injection rate. Without scaling, a strong linear correlation of pressure increase with injection rate was still observed.

At any dimensionless time during the process, the total pressure drop across the core is given by (Willhite 1986)

$$\Delta P_{t_D} = -\frac{q_t L}{KA}\left(\int_0^1 \frac{\mathrm{d}x_D}{\lambda_t}\right)_{t_D}, \quad \ldots\ldots\ldots\ldots\ldots\ldots\ldots (17)$$

where λ_t is the total fluid mobility at any instance. The results shown in Fig. 7b suggest that the incremental change in the integral term (equivalent to apparent viscosity, in nature) with injection time interval (Δt_D) is independent of the injection rate compared at the same dimensionless time.

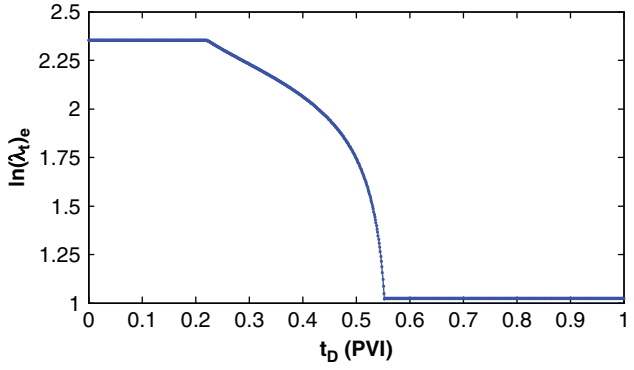

Fig. 8—Logarithm of total mobility at core exit face vs. dimensionless time in waterflooding test at 4.44 PV/D.

Regime III. Similar to Regime I, Regime III is also dominated by the capillarity at the core outlet face. A sharp capillary pressure gradient exists at this face because the capillary pressure is zero away from the core. This capillary pressure discontinuity results in capillary retention in the core. When water reaches the core outlet face, it invades high capillary pressure pore spaces in a hierarchical manner—with small pores being invaded first, as discussed by Chatzis and Dullien (1983). However, water cannot break through the invaded pores because water pressure is lower than the oil pressure in the amount equal to the capillary pressure at corresponding water saturation (at outlet face). Breakthrough occurs when the hydrodynamic pressure gradient overcomes the capillary pressure gradient at core outlet face. For a strongly water-wet fired Berea core, this condition occurs at the proximity of ROS when the capillary pressure becomes negligible. This explains why the oil production after water breakthrough was small, as shown in Fig. 4.

An important feature of the pressure signal in Regime III is the sudden change in the slope of pressure vs. time. The issue becomes determining what causes a sudden change in the pressure. The water phase accumulates over time at the core outlet face in the direction of reducing the capillary pressure. During this time, the saturation of water in the core changes accordingly. However, near breakthrough, the saturation does not change upon water injection, and it results in increase in pressure to enable breakthrough. After breakthrough, the core loses a part of driving force equal to imbibition capillary pressure, and the flow demands higher injection pressure accordingly.

We discuss the sudden pressure increase from a macroscale perspective by conducting the analysis of total mobility at the core outlet face. The natural logarithm of total fluid mobility at the outlet face is plotted vs. dimensionless time in **Fig. 8** for the waterflooding test conducted at 4.44 PV/D (Run 3 in Table 4). Initially, the logarithm of total mobility was constant at 2.35, corresponding to the mobility of oil phase because water had not reached the outlet face. After approximately 22% PVI, water reached the outlet face and the logarithm of total mobility decreased over time to unity at breakthrough (Regimes II, III). When water reaches the outlet face pore spaces, it invades the smaller pores first. These pores do not contribute much to flow of oil. But because the water stays stationary at the core outlet face, the fluid total mobility decreases. Larger pores become hierarchically invaded as the process progresses. These larger pores block a significant area for the flow of oil, and the total mobility significantly decreases up to breakthrough time because water does not flow. This sudden change in total mobility close to breakthrough resulted in sudden pressure increase, which is shown in Fig. 5 for injection rate of 4.44 PV/D. After breakthrough, the logarithm of

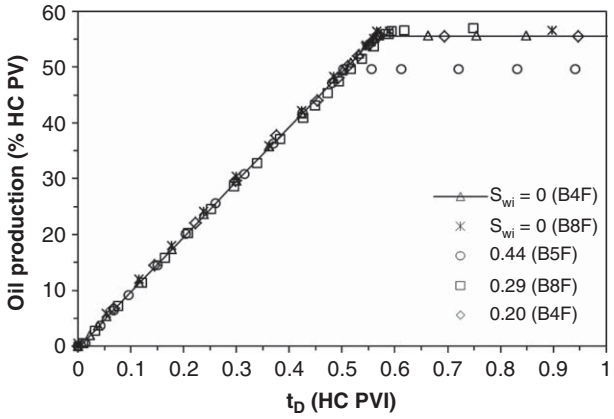

Fig. 9—Oil production vs. dimensionless time in waterflooding at 4.44 PV/D with and without initial water saturation.

total fluid mobility stayed constant at unity because the core outlet face stayed at ROS.

The total mobility in Fig. 8 is defined by the summation of water and oil mobilities:

$$\lambda_t = \lambda_w + \lambda_o = \left(\frac{k_{rw}}{\mu_w}\right) + \left(\frac{k_{ro}}{\mu_o}\right). \quad \ldots\ldots\ldots\ldots\ldots (18)$$

Regime IV. In this regime, water breakthrough has occurred; no oil was produced afterward for strongly water-wet cores. Therefore, the pressure was expected to stabilize after breakthrough for strongly water-wet cores (such as fired Berea core). The pressure in this regime is affected by the fluid properties, wettability, and injection rate. The dependence of endpoint relative permeability (and therefore, final stabilized pressure in waterflooding) on injection rate is well known. A pore-scale explanation of relative permeability dependency (and therefore, pressure drop) at residual saturation to injection rate is discussed by Morrow et al. (1983). They explained that when a drop of oil was trapped in a large water-wet pore, the applied pressure gradient might not be enough to mobilize the residual oil, but it might distort the blob shape in a way to plug the largest pore throat adjacent to the pore body. Therefore, it reduced the local permeability and gave rise to pressure drop across the core. At higher applied pressures, the residual oil droplets could have squeezed through the pore constriction, increasing the permeability to its value before pore blocking (after the residual oil was mobilized).

Effect of Initial Water Saturation. The effect of initial water saturation on waterflooding performance was investigated by conducting experiments with different initial water saturations in the core (Runs 7 through 9 in Table 4). Three initial water saturations of 0.20, 0.29 and 0.44 were investigated. These experiments were conducted in Cores B4F, B8F, and B5F, respectively. At the injection rate of 4.44 PV/D, poor recovery of brine was experienced from oilflooding of water-saturated cores (2.7% PV), which indicated viscous fingering in the core under these conditions. We flooded the water-saturated core with oil in increasing injection-rate steps until an initial water saturation of 0.44 was established. It was not possible to further reduce the initial water saturation by increasing the applied pressure gradient. To obtain lower initial water saturations (0.29 and 0.20), the temperature of the oven containing the core holder was raised to 100°C.

Fig. 9 summarizes the oil-production performance of fired Berea cores from waterflooding with and without the initial water saturation. Unlike previous plots, the *x*-axis shows dimensionless time in hydrocarbon PVI. The production that resulted in an initial water saturation of 0.44 is in line with literature data (Tang and Firoozabadi 2001); the oil recovery is expected to decrease with initial water saturation (Tang and Firoozabadi 2001). This is because the high capillary pressure continuum of pore spaces was already saturated with water before water injection starts. For $S_{wi} = 0.44$, the breakthrough occurred earlier, compared with the baseline experiments without initial water saturation. However, at lower initial water saturations ($S_{wi} = 0.29$ and 0.20 PV), there is not a significant difference between the recoveries of these two runs from their baseline experiments without initial water saturation, as seen in Fig. 9. Tang and Firoozabadi (2001) also observed a negligible difference in the waterflooding behavior of strongly water-wet cores with $S_{wi} = 0$ up to 0.21 PV; they found a small reduction in the final oil recovery by waterflooding at initial water saturation of 0.31 PV. In their experiments, they lowered the initial water saturation by applying vacuum to vaporize a portion of water. Note that for initial water saturations of 0.2 and 0.29 PV, waterflooding tests were conducted in two different cores (Cores B4F and B8F). A reference experiment was also conducted without the initial water saturation in the same core, and at the same injection rate to serve as reference. The results of waterflooding in Cores B4F and B8F without the initial water saturation are similar, which is expected because of the core similarities (they are obtained from a single batch). Furthermore, comparing the waterflooding in Core B4F with $S_{wi} = 0$ and 0.20 PV and that in Core B8F with $S_{wi} = 0$ and 0.29 PV demonstrated similar production behavior with and without the initial water saturation for these low initial water saturations. At the high initial water saturation (0.44 PV), the water is distributed as a thin film covering strongly water-wet grain surface roughness, and as water in the pore corner of fine grains (pore throats). There is a continuity of water-wetted surfaces along the core; however, when allowing for evaporation (either by heat or by applying vacuum), this continuity of water film may no longer exist, because some of the films will eventually dry out.

We show the ratio of ROS to initial oil saturation in the last column of Table 4. This ratio is in the range 0.43 to 0.45 for all runs except for Run 7. When the initial water saturation was lowered below that of immiscible displacement (by drying), the ratio S_{or}/S_{oi} behaved similar to that of dry cores as observed for Runs 8 and 9. The data of S_{or}/S_{oi} suggest the possibility that the initial oil in the core might have been disconnected by water imbibition during the aging. Note that when the injection pressure is eliminated (during aging), new capillary equilibrium will be held by water redistribution in the core.

The injection pressures at different initial water saturations are plotted in **Fig. 10.** The pressure vs. dimensionless time (in total PV injected) is shown in Fig. 10a. The rate of increase in pressure by water injection (Region II in Fig. 6) decreased with the initial water saturation. The stabilized pressure drop in Regime IV was also decreased by the increase in the initial water saturation. However, the pressure at no initial water saturation did not follow the same trend as the tests with the initial water saturation. The change in the permeability of the cores affects the pressure results. A dimensionless pressure is plotted in Fig. 10b vs. dimensionless time (in hydrocarbon PVI) to scale for permeability change. This figure shows a consistent trend when the initial water saturation increases. Note that the effective oil permeability was used for scaling. According to this figure, waterflooding with no initial water saturation gave the highest final scaled pressure. The rate of increase in pressure by injection was similar to the three cases with the initial water saturations of 0, 0.20, and 0.29, and it decreased for $S_{wi} = 0.44$. Comparing the two runs in Core B4F ($S_{wi} = 0$ and 0.20) showed similar capillary end effects with and without the initial water saturation. However, the capillary end effects were significantly reduced for the case with the initial water saturation of 0.44.

In agreement with production plots, the dimensionless-pressure behaviors at three initial water saturations of $S_{wi} = 0$, 0.20, and 0.29 had some similarities, whereas the pressure behavior was different at the highest initial water saturation. The endpoint relative permeability (and, therefore, final stabilized pressure drop in waterflooding in Fig. 6) is known to be significantly affected by the ROS (Morrow et al. 1983), which is different in the case of initial water saturation of 0.44 PV (as shown in Fig. 9). Therefore,

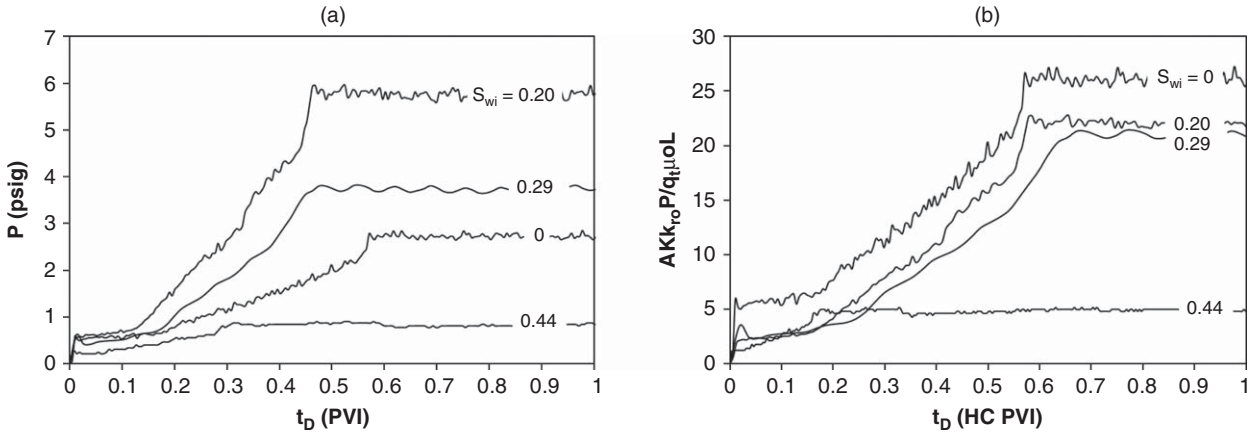

Fig. 10—Injection pressure vs. dimensionless time in waterflooding tests at 4.44 PV/D with and without the initial water saturation: (a) pressure and (b) dimensionless-pressure data.

pressure in Region IV is expected to be different for this case, compared with all the other runs. At zero initial water saturation, the residual oil forms in larger pores or as an oil blob extended in a cluster of large pores. Water cannot reach this continuum of larger pores during a waterflood, so it will not wet the surface of grains in some areas with low capillary pressure. On the other hand, when water initially wets the grain surfaces (for $S_{wi} = 0.44$), a continuum of wetting phase exists through the core at the time of breakthrough, even for the pores with residual oil. The presence of these continuous water films allows for transferring pressure (and momentum) through the wetting phase. In other words, the effective permeability to water is initially higher with the initial water saturation. This explains why the pressure attained in Region IV was the lowest for the highest initial water saturation. In other intermediate initial water saturations, some of the grains (with high capillary pressure) are initially wetted by the oil.

Simulation Results. We used the mathematical model to obtain the exponents of relative permeability n_w and n_o and k^0_{rw} for $S_{wi} = 0$. The experimental injection pressure and oil-production history were fitted to the model at each injection rate. The relative permeability exponents were obtained to be 1.500 ± 0.075 and 1.800 ± 0.075 for water and oil, respectively. The estimated water endpoint relative permeabilities k^0_{rw} were 0.08, 0.11, 0.14, and 0.15, respectively, at the corresponding injection rates of 2.2, 4.4, 11.1, and 22.2 PV/D. This rate dependency of endpoint relative permeability is explained in the work of Morrow et al. (1983). The endpoint relative permeability to oil was assumed to be unity because no initial water exists in the cores. The solver discretized the set of model equations along the spatial coordinate and integrated them over time. We have conducted grid sensitivity and used the grid sizes for the x_D and t_D to be 0.01.

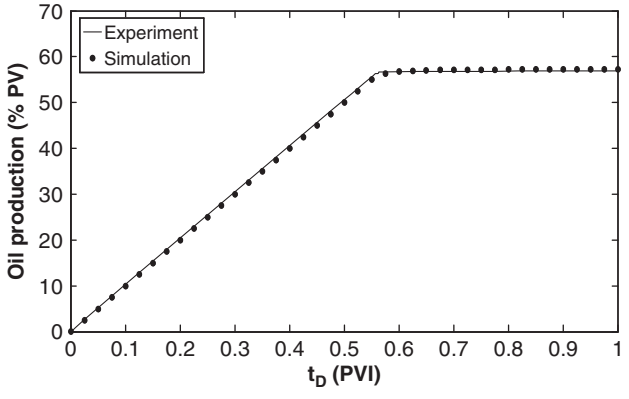

Fig. 11—Simulation and experimental results of oil production as a function of dimensionless time in waterflooding of *n*-C_7/brine system at 4.44 PV/D.

Fig. 11 compares the mathematical model and experimental results in estimating the oil production over time for a waterflooding test conducted at 4.44 PV/D at room temperature (Run 3 in Table 4). In general, the injection rate did not appreciably affect the oil-production performance of *n*-C_7/brine system in fired Berea cores, in the range of 2.2 to 22.2 PV/D. A good agreement was observed for oil recovery at all injection rates. We show only the results for 4.44-PV/D injection rate for brevity because the difference between the oil recoveries from simulation runs at different rates was small.

A comparison of pressure from experimental and simulation results is presented in **Figs. 12a through 12d** for injection rates in the range of 2.2 to 22.2 PV/D. As this figure shows, good agreement is observed between experimental and simulation results, except for the pressure behavior of Regime III in Fig. 12a. At lower injection rates, the extent of capillary pressure at the time of breakthrough was comparable with the net pressure drop at this time. For injection rate of 2.2 PV/D, a sudden change in pressure from 0.95 to 1.35 psig was observed at the time of breakthrough. This pressure increase is required because the core loses the imbibition capillary pressure as a part of driving force for flow. That the model did not fully describe the pressure behavior of Regime III may be because there is no continuum flow during this period of time.

The 1D saturation profiles along the core are shown at different injection times, and for different injection rates in **Figs. 13a through 13d.** The saturation profiles became more piston-like at higher injection rates, whereas capillarity tends to disperse the wetting phase in the core at lower injection rates, as seen in Fig. 13a. Furthermore, water reached the outlet side of the core faster at lower injection rates because of the contribution of spontaneous imbibition in saturation distribution along the core.

We have also used the mathematical model to obtain the exponents of relative permeability n_w and n_o and k^0_{rw} and k^0_{ro} for the run for $S_{wi} = 0.44$ (Run 7). There is good agreement between simulated and measured pressure profiles for $n_w = 1.4$, $n_o = 1.5$, $k^0_{rw} = 0.28$, and $k^0_{ro} = 0.74$. These parameters are within the range of expected values.

Conclusions

The following conclusions are drawn from this work:

- Four different regimes were identified in the injection-pressure profile (Fig. 6). Two regimes (Regimes I and III) were dominated by the inlet and outlet capillary end effects. In Region I, the injection pressure was constant because of the spontaneous-imbibition process. Region III was also governed by the capillary discontinuity of the core outlet, which showed a sudden pressure rise up to breakthrough time. Region II was governed

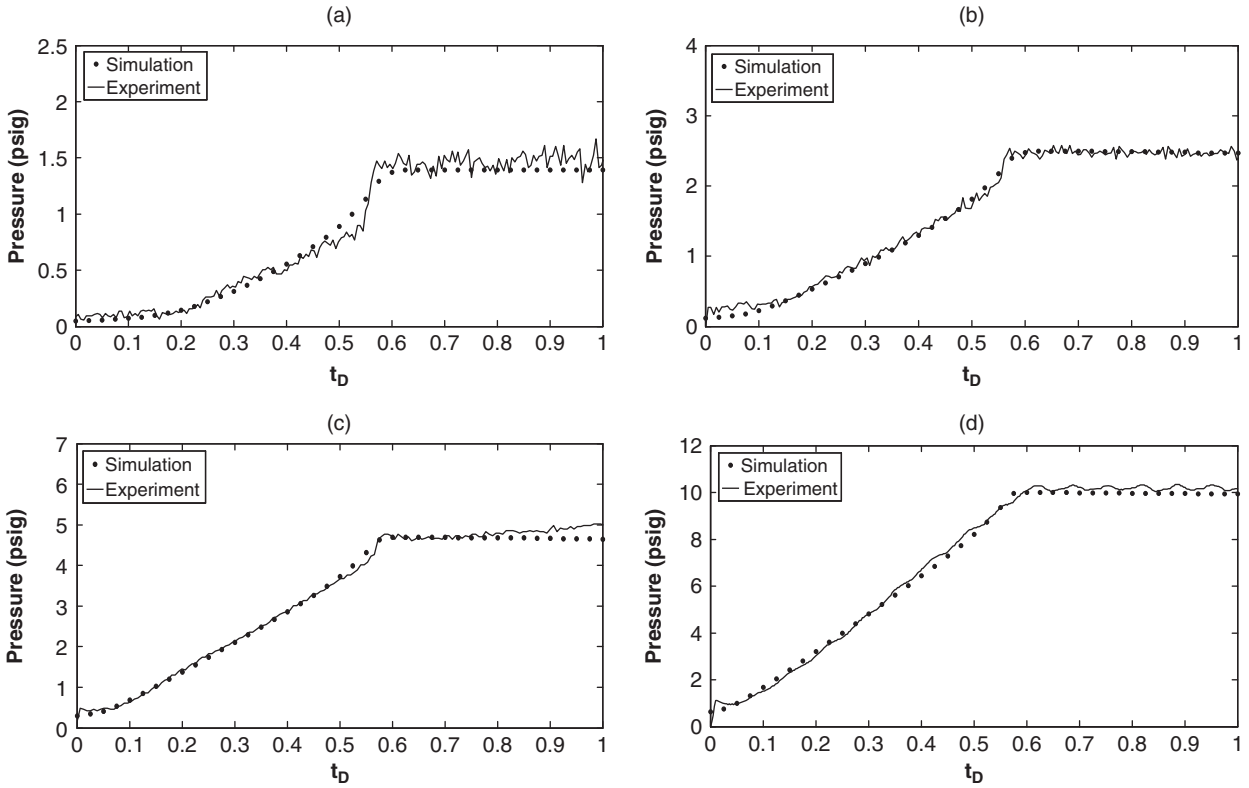

Fig. 12—Simulation and experimental results of injection pressure as a function of dimensionless time at different injection rates without the initial water saturation: (a) 2.22, (b) 4.44, (c) 11.11, and (d) 22.22 PV/D.

by viscous forces exhibited by the relative mobility of both phases, featuring a linear increase in the injection pressure up to proximity of breakthrough. In Region IV, pressure stabilized after breakthrough.

- The duration of constant pressure during the early time of waterflooding was affected by the injection rate; it was longer at low injection rates. The rate of increase in pressure in Regime II was also found to strongly correlate with the injection rate.
- No significant difference was observed in the oil-production performance by varying the injection rate by an order of magnitude in the range of 2.2 to 22.2 PV/D (equivalent to $Ca = 10^{-7}$ to 10^{-6}).

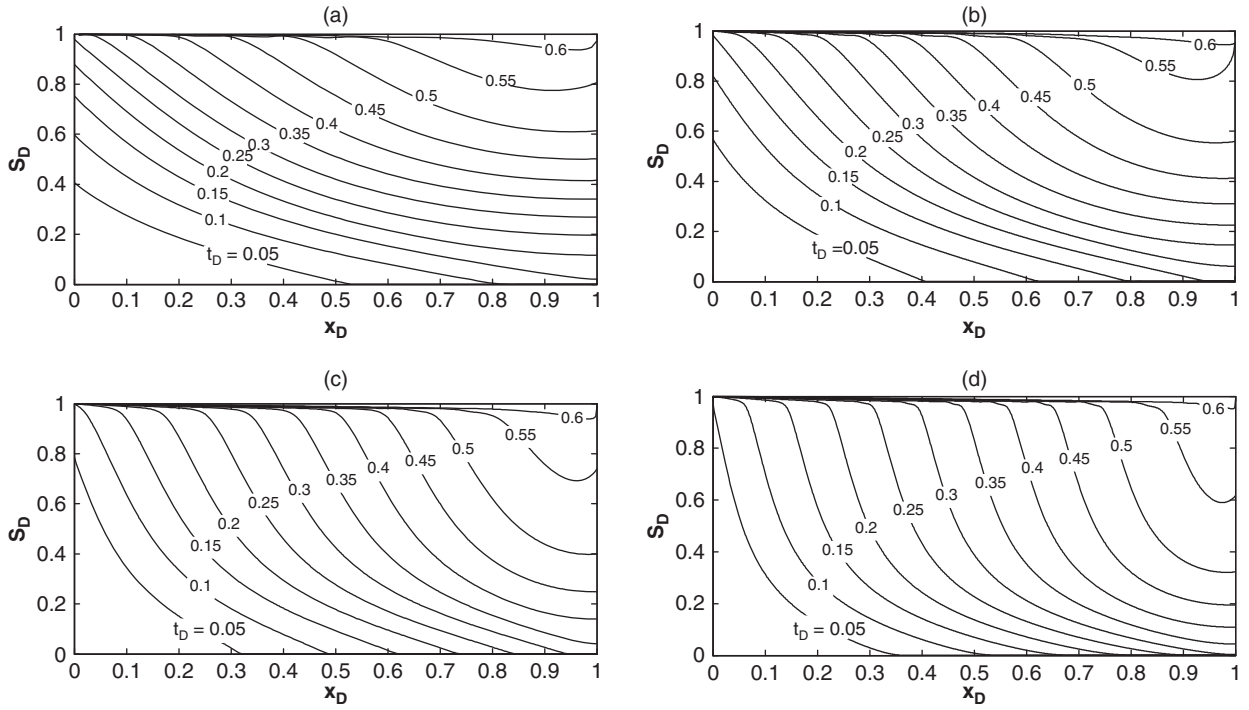

Fig. 13—Saturation profiles at different dimensionless times from simulation results at different injection rates without the initial water saturation: (a) 2.22, (b) 4.44, (c) 11.11, and (d) 22.22 PV/D.

- Varying the initial water saturation from 0 to 0.20 and at values of 0.29 and 0.44 PV showed that the effect of initial water saturation on pressure and production performance is more pronounced in high initial water saturation (0.44). Lower final oil-recovery factor was observed at high initial water saturation. Both the pressure at breakthrough and the rate of pressure increase over time were also lower at this level of initial water saturation compared with no initial water saturation. When decreasing the initial water saturation beyond that achieved in the oilflooding (by means of heating or by applying vacuum), the oil-production performance became similar to that of a core with no initial water saturation.
- The results from the mathematical model, including the capillary pressure, showed excellent agreement for oil production and pressure dynamics, except for the sudden pressure rise at the proximity of breakthrough. In the absence of in-situ saturation-profile measurements, we recommend to fit the model to the injection pressure rather than the oil-production history.

Nomenclature

a = capillary pressure model parameter, dyne/cm^2
A = cross-sectional area, cm^2
b = capillary pressure model parameter
c = capillary pressure model parameter, dyne/cm^2
Ca = capillary number
D = core diameter, cm
g = acceleration constant, cm/s^2
J = Leverett J-function
K = absolute permeability, cm^2
k_r^0 = endpoint relative permeability
L = core length, cm
n = relative permeability exponent
P = pressure, dyne/cm^2
q = flow rate, cm^3/s
S = saturation
t = time, seconds
u = darcy velocity, cm/s
x = horizontal spatial location, cm
α = phase, oil or water
γ = interfacial tension, dyne/cm
ζ = dimensionless number in model
η = dimensionless number in model
θ = contact angle, degrees
λ = fluid mobility, cm·s^2/dyne
μ = fluid viscosity dyne·s/cm^2
σ = surface tension, dyne/cm
ϕ = effective porosity

Subscripts

BKT = breakthrough
c = capillary
D = dimensionless
e = exit
i = initial
inj = injection
o = oil
ow = oil/water
or = residual oil
r = relative
w = water
t = total

Superscript

imb = imbibition

Acknowledgments

The support by the members of the consortium of the Reservoir Engineering Research Institute (RERI), Palo Alto, California, is greatly acknowledged. Nima Rezaei would like to thank Ioannis Chatzis of the University of Waterloo for his valuable and productive discussions.

References

Abrams, A. 1975. The Influence of Fluid Viscosity, Interfacial Tension, and Flow Velocity on Residual Oil Saturation Left by Waterflood. *SPE J.* **15** (5): 437–447. http://dx.doi.org/10.2118/5050-PA.

Agbalaka, C., Dandekar, A., Patil, S., et al. 2008. The effect of wettability on oil recovery: a review. Paper SPE 114496 presented at the SPE Asia Pacific Oil and Gas Conference and Exhibition, Perth, Australia, 20–22 October. http://dx.doi.org/10.2118/114496-MS.

Anderson, W. 1987a. Wettability Literature Survey Part 5: The Effects Of Wettability On Relative Permeability. *J. Pet. Tech.* **39** (11): 1453–1468. http://dx.doi.org/10.2118/16323-PA.

Anderson, W. 1987b. Wettability Literature Survey-Part 6: The Effects of Wettability on Waterflooding. *J. Pet. Tech.* **39** (12): 1605–1622. http://dx.doi.org/10.2118/16471-PA.

Ashraf, A., Hadia, N., Torsaeter, O., et al. 2010. Laboratory Investigation of Low Salinity Waterflooding as Secondary Recovery Process: Effect of Wettability. Paper SPE 129012 presented at SPE Oil and Gas India Conference and Exhibition, Mumbai, India, 20–22 January. http://dx.doi.org/10.2118/129012-MS.

Atkins, P. and Jones, L. 2007. *Chemical Principles: The Quest for Insight.* New York: W.H. Freeman & Co.

Bernard, G. 1967. Effect of Floodwater Salinity on Recovery Of Oil from Cores Containing Clays. Paper SPE 1725 presented at the SPE California Regional Meeting, Los Angeles, California, 26–27 October. http://dx.doi.org/10.2118/1725-MS.

Bolås, T. and Torsæter, O. 1995. Theoretical and Experimental Study of the Positive Imbibition Capillary Pressure Curves Obtained from Centrifuge Data. Oral presentation given at the 1995 International Symposium of the Society of Core Analysts, San Francisco, California, 12–14 September.

Boynton, R.S. 1980. *Chemistry and Technology of Lime and Limestone*. New York City, New York: John Wiley & Sons, Inc.

Brown, W. 1957. The Mobility of Connate Water During a Water Flood. *Trans. AIME* **210**: 190–195.

Buckley, J. and Liu, Y. 1998. Some Mechanisms of Crude Oil/Brine/Solid Interactions. *J. Pet. Sci. Eng.* **20** (3–4): 155–160. http://dx.doi.org/10.1016/S0920-4105(98)00015-1.

Carll, J.F. 1880. The Geology of the Oil Regions of Warren, Venango, Clarion and Butler Counties. *Second Geol. Survey of Pennsylvania Report 3* **482:** 263–269.

Catalan, L., Dullien, F. and Chatzis, I. 1994. The Effects of Wettability and Heterogeneities on the Recovery of Waterflood Residual Oil with Low Pressure Inert Gas Injection Assisted by Gravity Drainage. *SPE Advanced Technology Series* **2** (2): 140–149. http://dx.doi.org/10.2118/23596-PA.

Chalbaud, C., Lombard, J.M., Martin, F., et al. 2007. Two Phase Flow Properties of Brine-CO2 Systems in a Carbonate Core: Influence of Wettability on Pc and kr. Paper SPE 111420 presented at the SPE/EAGE Reservoir Characterization and Simulation Conference, Abu Dhabi, UAE, 28–31 October. http://dx.doi.org/10.2118/111420-MS.

Chatzis, I. and Dullien, F. 1983. Dynamic Immiscible Displacement Mechanisms in Pore Doublets: Theory Versus Experiment. *J. Colloid Interf. Sci.* **91** (1): 199–222. http://dx.doi.org/10.1016/0021-9797(83)90326-0.

Chatzis, I., Kuntamukkula, M. and Morrow, N. 1988. Effect of Capillary Number on the Microstructure of Residual Oil in Strongly Water-Wet Sandstones. *SPE Res Eval & Eng* **3** (3): 902–912. http://dx.doi.org/10.2118/13213-PA.

Chatzis, I. and Morrow, N. 1984. Correlation of Capillary Number Relationships for Sandstone. *SPE J.* **24** (5): 555–562. http://dx.doi.org/10.2118/10114-PA.

Chatzis, I., Morrow, N. and Lim, H. 1983. Magnitude and Detailed Structure of Residual Oil Saturation. *SPE J.* **23** (2): 311–326. http://dx.doi.org/10.2118/10681-PA.

Dawe, R., Wheat, M. and Bidner, M. 1992. Experimental Investigation of Capillary Pressure Effects on Immiscible Displacement in Lensed and Layered Porous Media. *Transport Porous Med.* **7** (1): 83–101. http://dx.doi.org/10.1007/BF00617318.

Dong, M., Dullien, F.A.L, Dai, L., et al. 2006. Immiscible Displacement in the Interacting Capillary Bundle Model Part II. Applications of

Model and Comparison of Interacting and Non-Interacting Capillary Bundle Models. *Transport Porous Med.* **63** (2): 289–304. http://dx.doi.org/10.1007/s11242-005-6530-4.

Dong, M., Dullien, F.L. and Zhou, J. 1998. Characterization of Waterflood Saturation Profile Histories by the 'Complete' Capillary Number. *Transport Porous Med.* **31** (2): 213–237. http://dx.doi.org/10.1023/A:1006565621860.

Dong, M. and Dullien, F. 1997. A New Model for Immiscible Displacement in Porous Media. *Transport Porous Med.* **27** (2): 185–204. http://dx.doi.org/10.1023/A:1006580207133.

Douglas J. Jr., Blair, P. and Wagner, R. 1958. Calculation of Linear Waterflood Behavior Including the Effects of Capillary Pressure. *Trans. AIME* **213:** 96–102.

Dullien, F. and Dong, M. 2002. The Importance of Capillary Forces in Waterflooding: An Examination of the Buckley-Leverett Frontal Displacement Theory. *J. Porous Media* **5** (1): 1–15.

Edmondson, T. 1965. Effect of Temperature on Waterflooding. *J. Cdn. Pet. Tech.* **4** (4): 236–242. http://dx.doi.org/10.2118/65-04-09.

Fried, A. N. 1954. *Effect of Oil Viscosity on the Recovery of Oil by Water Flooding*. San Francisco, CA: US Department of the Interior, Bureau of Mines.

Gharbi, R. and Peters, E.J. 1993. Scaling Coreflood Experiments to Heterogeneous Reservoirs. *J. Pet. Sci. Eng.* **10** (2): 83–95. http://dx.doi.org/10.1016/0920-4105(93)90033-B.

Hamon, G. and Vidal, J. 1986. Scaling-Up the Capillary Imbibition Process From Laboratory Experiments on Homogeneous and Heterogeneous Samples. Paper SPE 15852 presented at the European Petroleum Conference, London, United Kingdom, 20–22 October. http://dx.doi.org/10.2118/15852-MS.

Hirasaki, G. 1975. Sensitivity Coefficients for History Matching Oil Displacement Processes. *SPE J.* **15** (1): 39–49. http://dx.doi.org/10.2118/4283-PA.

Hirasaki, G. 1996. Dependence of Waterflood Remaining Oil Saturation on Relative Permeability, Capillary Pressure, and Reservoir Parameters in Mixed-Wet Turbidite Sands. *SPE Res Eval & Eng* **11** (2): 87–92. http://dx.doi.org/10.2118/30763-PA.

Hognesen, E., Strand, S. and Austad, T. 2005. Waterflooding of Preferential Oil-Wet Carbonates: Oil Recovery Related to Reservoir Temperature and Brine Composition. Paper SPE 94166 presented at the SPE Europec/EAGE Annual Conference, Madrid, Spain, 13–16 June. http://dx.doi.org/10.2118/94166-MS.

Huang, Y., Ringrose, P. and Sorbie, K. 1996. The Effects of Heterogeneity and Wettability on Oil Recovery from Laminated Sedimentary Structures. *SPE J.* **1** (4): 451–462. http://dx.doi.org/10.2118/30781-PA.

Huggett, R.J. 2007. *Fundamentals of Geomorphology*. New York City, New York: Routledge.

Jadhunandan, P. and Morrow, N. 1995. Effect of Wettability on Waterflood Recovery for Crude-Oil/Brine/Rock Systems. *SPE Res Eval & Eng* **10** (1): 40–46. http://dx.doi.org/10.2118/22597-PA.

Ju, B.S., Fan, T.L., Zhang, J.C., et al. 2006. Oil Viscosity Variation and Its Effects on Production Performance in Water Drive Reservoir. *Petroleum Exploration and Development* **33** (1): 99–102.

Kashchiev, D. and Firoozabadi, A. 2003. Analytical Solutions for 1D Countercurrent Imbibition in Water-Wet Media. *SPE J.* **8** (4): 401–408. http://dx.doi.org/10.2118/87333-PA.

Kelley, D. and Caudle, B. 1966. The Effect of Connate Water on the Efficiency of High-Viscosity Waterfloods. *J. Pet. Tech.* **18** (11): 1481–1486. http://dx.doi.org/10.2118/1615-PA.

Kennedy, H.T., Burja, E.O. and Boykin, R.S. 1955. An Investigation of the Effects of Wettability on Oil Recovery by Water flooding. *J. Phys. Chem.* **59** (9): 867–869. http://dx.doi.org/10.1021/j150531a015.

Kyte, J. and Rapoport, L. 1958. Linear Waterflood Behavior and End Effects in Water-Wet Porous Media. *J. Pet. Tech.* **10** (10): 47–50. http://dx.doi.org/10.2118/929-G.

Lager, A., Webb, K. and Black, C. 2007. Impact of Brine Chemistry on Oil Recovery. Oral presentation given at the 14th European Symposium on Improved Oil Recovery, Cairo, Egypt, 22–24 April.

Leverett, M. 1940. Capillary Behavior in Porous Solids. *Trans. AIME* **142** (1): 152–169. http://dx.doi.org/10.2118/941152-G.

Ma, S. and Morrow, N.R. 1994. Effect of Firing on Petrophysical Properties of Berea Sandstone. *SPE Form Eval* **9** (3): 213–218. http://dx.doi.org/10.2118/21045-PA.

Mai, A. and Kantzas, A. 2009. Heavy Oil Waterflooding: Effects of Flow Rate and Oil Viscosity. *J. Cdn. Pet. Tech.* **48** (3): 42–51. http://dx.doi.org/10.2118/09-03-42.

McDougall, S. and Sorbie, K. 1993. The Combined Effect of Capillary and Viscous Forces on Waterflood Displacement Efficiency in Finely Laminated Porous Media. Paper SPE 26659 presented at the SPE Annual Technical Conference and Exhibition, Houston, Texas, 3–6 October. http://dx.doi.org/10.2118/26659-MS.

Melrose, J. and Melrose, J. 1974. Role of Capillary Forces In Detennining Microscopic Displacement Efficiency For Oil Recovery By Waterflooding. *J. Cdn. Pet. Tech.* **13** (4): 54–62. http://dx.doi.org/10.2118/74-04-05.

Morrow, N. 1979. Interplay of Capillary, Viscous And Buoyancy Forces In the Mobilization of Residual Oil. *J. Cdn. Pet. Tech.* **18** (3): 35–46. http://dx.doi.org/10.2118/79-03-03.

Morrow, N., Lim, H. and Ward, J. 1986. Effect of Crude-Oil-Induced Wettability Changes on Oil Recovery. *SPE Form Eval* **1** (1): 89–103. http://dx.doi.org/10.2118/13215-PA.

Morrow, N.R., Chatzis, I., and Lim, H. 1983. Relative permeabilities at reduced residual saturations. Presented at the 34th Petroleum Society of CIM Annual Technical Meeting, Banff, Canada, 10–13 May. OSTI ID: 6143857.

Morrow, N.R., Tang, G., Valat, M., et al. 1998. Prospects of Improved Oil Recovery Related to Wettability and Brine Composition. *J. Pet. Sci. Eng.* **20** (3–4): 267–276. http://dx.doi.org/10.1016/S0920-4105(98)00030-8.

Mungan, N. 1971. Improved Waterflooding Through Mobility Control. *Can. J. Chem. Eng.* **49** (1): 32–37. http://dx.doi.org/10.1002/cjce.5450490107.

Oseto, K., Al-Amoudi, A. and Suzuki, M. 2006. Comprehensive Approach of Core Analysis to Predict Waterflooding Performance in a Heterogeneous Carbonate Reservoir, Offshore Abu Dhabi. Paper SPE 101287 presented at the Abu Dhabi International Petroleum Exhibition and Conference, Abu Dhabi, UAE, 5–8 November. http://dx.doi.org/10.2118/101287-MS.

Parsaei, R. and Chatzis, I. 2011. Experimental Investigation of Production Characteristics of the Gravity-Assisted Inert Gas Injection (GAIGI) Process for Recovery of Waterflood Residual Oil: Effects of Wettability Heterogeneity. *Energ. Fuel.* **25** (5): 2088–2089. http://dx.doi.org/10.1021/ef200098y.

Perkins, F. Jr. 1957. An Investigation of the Role of Capillary Forces in Laboratory Water Floods. *J. Pet. Tech.* **9** (11): 49–51. http://dx.doi.org/10.2118/840-G.

Pooladi-Darvish, M. and Firoozabadi, A. 2000. Cocurrent and Countercurrent Imbibition in a Water-Wet Matrix Block. *SPE J.* **5** (1): 3–11. http://dx.doi.org/10.2118/38443-PA.

Rapoport, L.A. and Leas, W.J. 1953. Properties of Linear Waterfloods. *J Pet Technol* **5** (5): 139–148. SPE-213-G. http://dx.doi.org/10.2118/213-G.

Rezaei, N. and Chatzis, I. 2011. Characterization of Heterogeneities in Porous Media Using Constant Rate Air Injection Porosimetry. *J. Pet. Sci. Eng.* **79** (3–4): 113–124. http://dx.doi.org/10.1016/j.petrol.2011.08.019.

Ruth, D.W., Li, Y., Mason, G., et al. 2007. An Approximate Analytical Solution for Counter-Current Spontaneous Imbibition. *Transport Porous Med.* **66** (3): 373–390. http://dx.doi.org/10.1007/s11242-006-0019-7.

Ruth, D. and Arthur, J. 2011. A Revised Analytic Solution to the Linear Displacement Problem Including Capillary Pressure Effects. *Transport Porous Med.* **86** (3): 881–894. http://dx.doi.org/10.1007/s11242-010-9662-0.

Sharma, M. and Filoco, P. 2000. Effect of Brine Salinity and Crude-Oil Properties on Oil Recovery and Residual Saturations. *SPE J.* **5** (3): 293–300. http://dx.doi.org/10.2118/65402-PA.

Shaw, J., Churcher, P. and Hawkins, B. 1991. The Effect of Firing on Berea Sandstone. *SPE Form Eval* **6** (1): 72–78. http://dx.doi.org/10.2118/18463-PA.

Smith, J., Chatzis, I. and Ioannidis, M. 2005. A New Technique to Measure the Breakthrough Capillary Pressure. *J. Cdn. Pet. Tech.* **44** (11): 25–31. http://dx.doi.org/10.2118/05-11-01.

Tang, G.Q. and Firoozabadi, A. 2001. Effect of Pressure Gradient and Initial Water Saturation on Water Injection in Water-Wet and Mixed-Wet Fractured Porous Media. *SPE Res Eval & Eng* **4** (6): 516–524. http://dx.doi.org/10.2118/74711-PA.

Tang, G.Q. and Morrow, N. 1997. Salinity, Temperature, Oil Composition, and Oil Recovery by Waterflooding. *SPE Res Eval & Eng* **12** (4): 269–276. http://dx.doi.org/10.2118/36680-PA.

Tie, H., Tong, Z. and Morrow, N.R. 2003. The Effect of Different Crude Oil/Brine/Rock Combinations on Wettability through Spontaneous Imbibition. Oral presentation given at the International Symposium of the Society of Core Analysts, Pau, France, 21–24 September.

Torabi, F., Yadali Jamaloei, B., Zarivnyy, O., et al. 2010. Effect of Oil Viscosity, Permeability and Injection Rate on Performance of Waterflooding, CO2 Flooding and WAG Processes on Recovery of Heavy Oils. Paper SPE 138188 presented at the Canadian Unconventional Resources and International Petroleum Conference, Calgary, Alberta, Canada, 19–21 October. http://dx.doi.org/10.2118/138188-MS.

Wang, J. and Dong, M. 2009. Optimum Effective Viscosity of Polymer Solution for Improving Heavy Oil Recovery. *J. Pet. Sci. Eng.* **67** (3): 155–158. http://dx.doi.org/10.1016/j.petrol.2009.05.007.

Whitaker, S. 1986. Flow in porous media II: The Governing Equations for Immiscible, Two-Phase Flow. *Transport Porous Med.* **1** (2): 105–125. http://dx.doi.org/10.1007/BF00714688.

Willhite, G.P. 1986. Waterflooding. Richardson, Texas: Textbook Series, SPE.

Worthington, A. 1978. A Technique for Detecting Incomplete Saturation of Cores. *J. Pet. Tech.* **30** (12): 1716–1717. http://dx.doi.org/10.2118/6982-PA.

Wu, S. and Firoozabadi, A. 2011. Effects of Firing and Chemical Treatments on Berea Permeability and Wettability. *Energ. Fuel.* **25** (1): 197–207. http://dx.doi.org/10.1021/ef1007984.

Wu, T., Zhang, X., Li, B. et al. 2011. Effect of wettability of low-permeability sandstone on waterflooding and ASP flooding recovery (in Chinese). *Fault-Block Oil & Gas Field* (2011-03).

Yildiz, H., Valat, M. and Morrow, N. 1999. Effect of Brine Composition on Wettability and Oil Recovery of a Prudhoe Bay Crude Oil. *J. Cdn. Pet. Tech.* **38** (1): 26–31. http://dx.doi.org/10.2118/99-01-02.

Yildiz, H.O. and Morrow, N.R. 1996. Effect of Brine Composition on Recovery of Moutray Crude Oil by Waterflooding. *J. Pet. Sci. Eng.* **14** (3–4): 159–168. http://dx.doi.org/10.1016/0920-4105(95)00041-0.

Yortsos, Y. and Fokas, A. 1983. An Analytical Solution for Linear Waterflood Including the Effects of Capillary Pressure. *SPE J.* **23** (1): 115–124. http://dx.doi.org/10.2118/9407-PA.

Yu, C., Li, M., Qiao, G., et al. 2009. Vertically Heterogeneous Reservoir Waterflooding Oil Test. *Journal of Southwest Petroleum University (Science & Technology Edition)* **31** (1): 84–86. http://dx.doi.org/10.3863/j.issn.1674-5086.2009.01.021.

Zhang, Y., Xie, X. and Morrow, N. 2007. Waterflood Performance by Injection of Brine with Different Salinity for Reservoir Cores. Paper SPE 109849 presented at the SPE Annual Technical Conference and Exhibition, Anaheim, California, 11–14 November. http://dx.doi.org/10.2118/109849-MS.

Zhou, X., Morrow, N. and Ma, S. 2000. Interrelationship of Wettability, Initial Water Saturation, Aging Time, and Oil Recovery by Spontaneous Imbibition and Waterflooding. *SPE J.* **5** (2): 199–207. http://dx.doi.org/10.2118/62507-PA.

Zhou, X.-m., Torsater, O., Xie, X. and Morrow, N.R. 1995. The Effect of Crude-Oil Aging Time and Temperature on the Rate of Water Imbibition and Long-Term Recovery by Imbibition. *SPE Form Eval* **10** (4): 259–266. http://dx.doi.org/10.2118/26674-PA.

Zhou, Y., Li, Y. and Wang, D.P. 2008. Research on Water Flooding Effect Improved by Vectorial Well Arrangement for Reservoirs with Permeability Heterogeneity in Plane. *Yantu Lixue (Rock and Soil Mechanics)* **29** (1): 135–139.

SI Metric Conversion Factors

cp × 1*	E−03 = Pa·s
darcy × 9.869233	E−01 = μm^2
dyne × 1*	E−02 = mN
psi × 6.894757	E+00 = kPa

*Conversion factor is exact.

Nima Rezaei holds a bachelor's degree in chemical engineering (process design) from Sharif University of Technology, Tehran, Iran; a master's degree in chemical engineering from Shiraz University, Shiraz, Iran; and a PhD degree in chemical engineering from the University of Waterloo. He has been a visiting scholar at the University of Waterloo and a post-doctoral fellow at RERI. Rezaei's research interests are in conventional and heavy-oil recovery processes, flow visualization in porous media, pore-structure characterization, and thermodynamics of hydrocarbon reservoirs.

Abbas Firoozabadi conducts research at RERI and teaches at Yale University. His main research interests are in bulk-phase, irreversible, and interfacial thermodynamics, and physics and mathematics of hydrocarbon reservoirs and production. Firoozabadi's current research focus is on shale-gas reservoirs, molecular modeling of petroleum fluids in relation to flow assurance and emulsions, and heavy oils. His honors/awards include the SPE/AIME Anthony Lucas Gold Medal and membership in the US National Academy of Engineering. Firoozabadi holds a bachelor's degree in natural-gas engineering from Abadan Institute of Technology, Abadan, Iran, and master's and PhD degrees, both in gas engineering, from the Illinois Institute of Technology.